Removal of PsaF Alters Forward Electron Transfer in Photosystem I: Evidence for Fast Reoxidation of Q_K-A in Subunit Deletion Mutants of *Synechococcus* sp. PCC 7002[†]

Art van der Est,*[,‡] Alfia I. Valieva,[‡,§] Yuri E. Kandrashkin,[‡,||] Gaozhong Shen,[⊥] Donald A. Bryant,[⊥] and John H. Golbeck[⊥]

Department of Chemistry, Brock University, 500 Glenridge Avenue, St. Catharines, Ontario, Canada L2S 3A1, Kazan Institute of Biochemistry and Biophysics and Kazan Physical Technical Institute, RAS, Kazan, Russia, and Department of Biochemistry and Molecular Biology, The Pennsylvania State University, University Park, Pennsylvania 16802

Received August 11, 2003; Revised Manuscript Received December 5, 2003

ABSTRACT: Recent studies of point mutations in photosystem I have suggested that the two kinetic phases of phylloquinone reoxidation represent electron transfer in the two branches of cofactors. This interpretation implies that changes in the relative amplitudes of the two kinetic phases represent a change in the extent of electron transfer in the two branches. Using time-resolved electron paramagnetic resonance (EPR), this issue is investigated in subunit deletion mutants of *Synechococcus* sp. PCC 7002. The spin-polarized EPR signals of $P_{700}^+A_1^-$ and $P_{700}^+FeS^-$, both at room temperature and in frozen solution, are altered by deletion of PsaF and/or PsaE, and the differences from the wild type are much more pronounced in PS I complexes isolated from the mutants using Triton X-100 rather than *n*-dodecyl β-D-maltopyranoside. The changes in the transient EPR data for the mutant complexes are consistent with a significant fraction of reaction centers showing (i) faster electron transfer from A_1^- to F_X, (ii) slower forward electron transfer from A_0^- to A_1, and (iii) slightly altered quinone hyperfine couplings, possibly as a result of a change in the hydrogen bonding. The fraction of fast electron transfer and its dependence on the isolation procedure are estimated approximately from simulations of the room temperature EPR data. The results are discussed in terms of possible models for the electron transfer. It is suggested that the detergent-induced fraction of fast electron transfer is most likely due to alteration of the environment of the quinone in the PsaA branch of cofactors and is not the result of a change in the directionality of electron transfer.

According to the identity of their terminal acceptors, photosynthetic reaction centers are divided into two classes referred to as type I and type II. The general arrangements of the cofactors in the electron-transfer chain are similar in type I (photosystem I (PS I)[1] and reaction centers of green sulfur bacteria and heliobacteria) and in type II (photosystem II (PS II) and purple bacteria) reaction centers. Both types have two nearly symmetric branches of acceptors extending across the membrane from the primary donor to a mobile electron carrier on the acceptor side. However, the nature of the mobile acceptor is considerably different in the two types of reaction centers. In type II, the quinone associated with the B-branch of cofactors acts as the terminal acceptor and as a mobile electron carrier. Because of this, the initial charge separation is strongly biased toward the A-branch of cofactors. In contrast, in type I reaction centers such as PS I, the two branches converge at the acceptor F_X, and as a result, the mobile electron carrier, ferredoxin or flavodoxin, is not associated with either of the two branches. This raises the question of whether both of the quinones are active in electron transfer in PS I or one of the quinones plays a different, unrecognized role.

Recently, this question has been addressed by studying the kinetics of quinone reoxidation using various forms of time-resolved spectroscopy (*1*−*5*). In particular, optical studies of the absorbance changes in the near-UV have shown that in many species the electron-transfer kinetics from A_1 to F_X has two components that can be affected by a number of factors (see refs *6* and *7* for reviews). In spinach PS I complexes, the reoxidation of A_1 has been found to occur with $t_{1/2}$ values of about 25 and 150 ns (*8*), while in cyanobacterial PS I, initial measurements suggested that the kinetics were monophasic with a $t_{1/2}$ of about 200 ns (*9*−*11*). However, later experiments with higher time resolution revealed a minor fraction with a $t_{1/2}$ of 6.6 ns (*12*). The slow

[†] This work was supported by grants to A.v.d.E. from the NSERC, CFI, and OIT and to J.H.G. (MCB-0117079) and to D.A.B. (MCB-0077586) from the U.S. National Science Foundation.

* To whom correspondence should be addressed. Phone: 1 (905) 688-5550. Fax: 1 (905) 682-9020. E-mail: avde@brocku.ca.

[‡] Brock University.

[§] Kazan Institute of Biochemistry and Biophysics, RAS.

[||] Kazan Physical Technical Institute, RAS.

[⊥] The Pennsylvania State University.

[1] Abbreviations: PS I, photosystem I; PS II, photosystem II, P_{700}, primary donor in PS I, A_0, primary chlorophyll acceptor in PS I; A_1, quinone acceptor in PS I; F_X, F_A, and F_B, iron−sulfur clusters in PS I; FeS, unpecified iron−sulfur cluster; PsaA, PsaB, etc., protein subunits of the PS I complex; Q_K-A, Q_K-B, phylloquinones bound to PsaA and PsaB; β-DM, *n*-dodecyl-β-D-maltopyranoside; WT, wild type; Δ*psaE*, Δ*psaF*, Δ*psaE*/Δ*psaF*, subunit deletion mutants; EPR, electron paramagnetic resonance; ENDOR, electron nuclear double resonance; E, emission; A, absorption.

10.1021/bi035431j CCC: $27.50
Published on Web 01/16/2004

kinetic phase is strongly temperature dependent (*13*), while the fast phase is virtually independent of temperature (*14*). Below the glass transition temperature of the protein, forward transfer past A_1 is blocked in approximately half of the reaction centers and stable formation of $P^+(F_A/F_B)^-$ occurs in the other half. At present it is unknown whether a correlation exists between the two fractions observed at low temperature and the two kinetic phases observed at higher temperature. An interesting feature of the two phases is that in spinach the relative amplitudes are very dependent on the method used to isolate PS I (*8*); a larger fraction of fast electron transfer is observed in complexes isolated using strong detergents. When Triton X-100 and β-mercaptoethanol are used, the fast phase dominates, while milder treatments give roughly equal amounts of the two phases, and when a Yeda press is used (i.e., no detergent), the fast kinetic phase is found to account for only 30% of the electron transfer. These results suggest that the fast phase might be a preparation-induced artifact. However, Joliot and Joliot (*15*) recently used optical spectroscopy with nanosecond time resolution to study the rate of forward electron transfer from A_1 to F_X in whole cells of a mutant strain of *Chlorella sorokiniana* lacking PS II and the peripheral antennae. They observed two phases with approximately equal amplitudes and $t_{1/2}$ values of 18 and 160 ns, clearly showing that the biphasic kinetics is an inherent property of PS I electron transfer and not a preparation-induced artifact.

Two hypotheses have been proposed to explain the origin of the two kinetic phases of quinone reoxidation (*2*, *15*). The first hypothesis suggests that the two kinetic phases represent electron transfer in the two branches of cofactors, while the second hypothesis assigns the two phases to two populations of PS I that differ structurally. The bidirectional model is supported primarily by point mutation studies of the eukaryote *Chlamydomonas reinhardtii* (*1*−*3*). These studies involved mutation of the tryptophan residue present in both branches, which is π-stacked with the respective phylloquinone. Mutation of the tryptophan on the PsaB side affects only the fast component, slowing the half-life of electron transfer from ∼20 to 73 ns, whereas the corresponding mutation on the PsaA side affects only the slower component, slowing it from ∼200 to ∼490 ns. Combined mutations in both sides alter both the fast and slow kinetic components. A more extensive study of mutants of the cyanobacterium *Synechocystis* sp. PCC 6803 (*4*, *5*) shows similar trends. The slow kinetic phase could clearly be associated with the PsaA branch of cofactors, while the correlation between mutations in the PsaB branch and changes in the fast kinetic phase, although present, was not as strong. Electron transfer along the PsaA branch is supported by low temperature and time-resolved EPR data (*1*, *5*) and is consistent with earlier photoaccumulation studies on subunit deletion mutant strains of *Synechococcus* sp. PCC 7002 (*16*). In the latter, it was shown that when the *psaE* and *psaF* genes were deleted and Triton X-100 was used to solubilize PS I, A_0^- was photoaccumulated at the expense of A_1^-. PsaE and PsaF were the only subunits for which such an effect was observed, and these subunits are located on the stromal side of the membrane on one side of the PS I complex. It was therefore suggested that the EPR-visible A_1^- signal is produced by the quinone[2] in the branch associated with the subunit closest to PsaE and PsaF (*17*). The difference in photoaccumulation behavior was explained by postulating that, in the absence of PsaE and PsaF, the detergent is able to open a water channel to the quinone, allowing it to be protonated and hence doubly reduced (*16*). This, in turn, allows A_0^- to be photoaccumulated. Although the quinone associated with the branch closer to PsaF was implicated, it was not known at the time which of the two subunits, PsaA or PsaB, corresponded to this branch. With the determination of the X-ray structure at 2.5 Å resolution, it is now known that the PsaA branch is closer to PsaF. This asymmetry in the location of the subunits is displayed in Figure 1, which shows two different views of the PS I complex that highlight the relative positions of the cofactor branches and the PsaE and PsaF subunits. The views, approximately along the membrane normal (crystallographic *c*-axis) from the stromal side of the membrane and parallel to the membrane plane, illustrate most clearly that these two subunits are much closer to the PsaA branch than the PsaB branch.

These results raise a number of interesting issues. In the unidirectional model of electron transfer, a change in the ratio of the two phases implies a change in the relative amounts of the two conformations associated with the two phases of electron transfer. In the bidirectional model, it implies a change in the fraction of electrons that are transferred along the two branches. Thus, the results showing that the use of strong detergents increases the amount of fast electron transfer in spinach preparations (*8*) imply that the detergent either changes the conformation of the protein near the active quinone or increases the fraction of electrons that are transferred along the PsaB branch. In the latter case, the detergent would need to affect P_{700} and/or A_0 because the ratio of electron transfer along the two branches is determined during the initial charge separation. Thus, a better understanding of the detergent effects on electron transfer in PS I should provide additional information for distinguishing between the two possible models.

In spinach PS I preparations, strong detergent treatments lead to reduced amounts of proteins of masses of 8, 16.5, and 20−22 kDa (*18*), a molecular mass range which includes the PsaE, PsaF, and PsaD proteins. Since these types of preparations typically show larger amounts of fast electron transfer to F_X, it is possible that the change in the ratio of the two phases is related to the loss of the peripheral subunits. Here, we investigate this possibility by studying the electron-transfer kinetics in peripheral subunit deletion mutants of cyanobacteria that show altered photoaccumulation behavior when PS I is isolated using Triton X-100. The motivation for these experiments is to test the proposal (*16*) that the combined effects of the detergent and mutation alter the protein environment of the quinone associated with the PsaA branch by correlating the changes in the photoaccumulation behavior with changes in the electron-transfer kinetics.

We use transient EPR spectroscopy for these experiments because it allows both the electron-transfer kinetics and the interaction of the quinone with its environment to be studied simultaneously (see refs *19*−*25* for a series of reviews). A

[2] *Synechococcus* sp. PCC 7002 has been shown to contain menaquinone-4 rather than phylloquinone (Y. Sakuragi and D. A. Bryant, unpublished results).

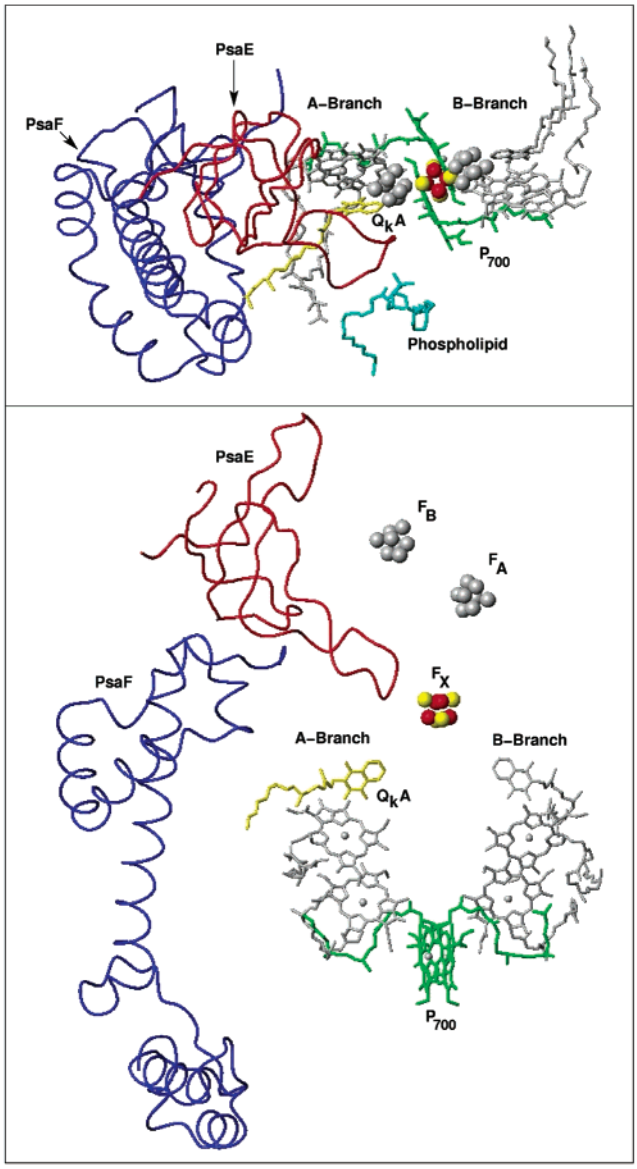

FIGURE 1: Location of the PsaE and PsaF subunits in PS I from the 2.5 Å resolution X-ray structure (*69*) (PDB entry **1JB0**). The complex is shown as viewed from two different perspectives. Top: view from the stromal side of the membrane along a direction roughly parallel to the membrane normal. Bottom: view from a direction roughly parallel to the membrane plane. The backbones of the PsaE and PsaF proteins are shown along with the electron-transfer cofactors. The figure was constructed using the program MOLMOL (*83*).

potential drawback of this method is that the spectrometer response time is typically ~50 ns and hence too slow to directly resolve fast electron-transfer steps. However, the presence of a short-lived precursor can be revealed indirectly through its influence on the spin polarization of subsequent radical pairs (*26*−*30*). This technique has been well established by studying the electron transfer from pheophytin to the quinone in modified reaction centers of purple bacteria (*27*, *28*, *31*−*36*). However, until fairly recently, similar studies in PS I were hampered by the lack of reliable magnetic interaction parameters, distances, and geometries for the cofactors. Over the past several years these parameters have become available from studies using high-field EPR (*37*−*41*), echo envelope modulation (*42*−*48*), pulsed and CW-ENDOR (*49*−*54*), quantum beats (*55*, *56*), and PS I single crystals (*43*, *57*−*61*). Recently, we investigated the room temperature polarization patterns of the sequential radical pair states $P_{700}{}^+A_1{}^-$ and $P_{700}{}^+FeS^-$ in cyanobacteria and showed that they are reproduced very well in simulations in which all of the necessary parameters are fixed using independent experimental data (*30*, *62*). These simulations are simplified by the fact that the small amplitude and short lifetime of the fast phase of electron transfer from $A_1{}^-$ to F_X in cyanobacteria make its contribution to the polarization patterns very small. However, this fraction can also be taken into account as shown by corresponding simulations of PS I from *C. rheinhardtii* in which a significant influence of the fast phase is observed (*63*). In native PS I preparations, the primary radical pair is too short-lived to have a significant effect on the spin polarization. However, in green sulfur bacteria and heliobacteria, the lifetime of $P^+A_0{}^-$ is more than an order of magnitude longer and effects similar to those observed in modified purple bacterial reaction centers (*27*, *28*, *31*−*36*) are seen (*64*). Again, the polarization patterns can be reproduced by taking the spin dynamics into account and by assuming a reasonable set of magnetic parameters (*62*, *65*).

All of these studies show that transient EPR is sensitive to the presence of short-lived precursors, and in well-characterized systems such as PS I and purple bacterial reaction centers, it can be used to estimate properties of such precursors even though they are not resolved kinetically. Here, we use this approach to investigate the influence of the deletion mutations and detergent isolation on the electron-transfer kinetics in cyanobacterial PS I. It is important to stress that this method can be expected to give accurate qualitative information about changes in the electron-transfer kinetics but not numerical values of the lifetimes of the short-lived radical pairs. We will show that the combined effect of deletion of PsaE and PsaF and isolation of PS I using Triton X-100 is to induce a much larger fraction of fast electron transfer to the iron sulfur clusters. Because PsaE and PsaF are located close to PsaA, we propose that this is due to changes in the electron transfer in the PsaA branch of cofactors and not due to electrons being redirected along the PsaB branch.

MATERIAL AND METHODS

Mutant strains of *Synechococcus* sp. PCC 7002 devoid of selected peripheral photosystem I subunits were prepared and grown as described in ref *16*. Three mutants were studied in which (i) the *psaE* gene was interrupted (Δ*psaE*), (ii) the *psaF* gene was interrupted (Δ*psaF*), and (iii) the *psaE* gene and the *psaF* gene were both interrupted (Δ*psaE*/Δ*psaF*). PS I trimers from wild-type and mutant strains were isolated using either 30 mM *n*-dodecyl-*β*-D-maltopyranoside (*β*-DM) or 1% (v/v) Triton X-100 to solubilize the thylakoid membranes as described previously (*16*). Trimeric PS I complexes were prepared at a chlorophyll concentration of 1.5−2 mg mL^{-1} in 50 mM Tris, pH 6.8, containing 15% (v/v) glycerol and 0.03% (w/v) *β*-DM or 1% (v/v) Triton X-100. To reduce P700, 5 *μ*M phenazine methosulfate (PMS) and 20 mM sodium ascorbate were added to the PS I complexes prior to the measurements.

Transient EPR time/field data sets were recorded at both room temperature and 135 K using a modified Bruker ER

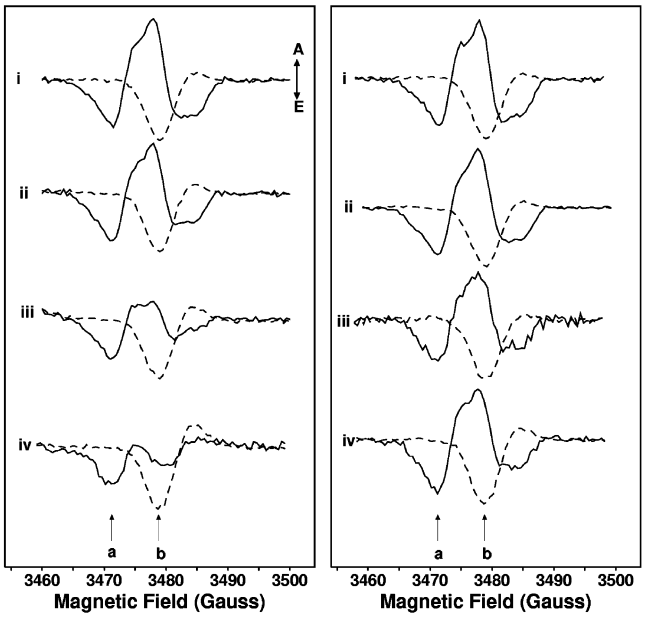

FIGURE 2: Room temperature transient EPR spectra of PS I complexes from the wild type and mutants lacking PsaE and/or PsaF. Left: PS I complexes isolated using Triton X-100. Right: PSI complexes isolated using β-DM. From top to bottom (i) wild type, (ii) Δ*psaE* mutant, (iii) Δ*psaF* mutant, (iv) Δ*psaE*/Δ*psaF* double mutant. The data are plotted such that absorptive signals (A) are positive and emissive signals (E) are negative. The two arrows labeled a and b indicate the positions of the transients shown in Figure 3. The spectra have been extracted from the data sets by integrating the signal intensity in time windows centered at 100 ns (solid line) and 1.2 μs (dashed line) after the laser flash. For the wild-type PS I complex, the solid curves are dominated by $P_{700}^+A_1^-$ while the dashed curves are due to $P_{700}^+F_X^-$.

200D-SRC X-band spectrometer which is described in detail elsewhere (*5*, *66*).

RESULTS

Room Temperature Transient EPR Results. Figure 2 shows room temperature, spin-polarized transient EPR spectra of PS I from the mutants and wild type. The spectra are taken at 100 ns (solid curves) and 1.2 μs (dashed curves) after the laser flash, and the two arrows labeled a and b indicate the field positions corresponding to the transients shown in Figure 3. Figures 2 and 3 also show a comparison of transients from PS I complexes isolated using Triton X-100 and β-DM displayed on the left and right, respectively. In all of the figures, positive signals represent absorptive spin polarization (A) and negative signals represent emissive polarization (E). As can be seen in Figure 2 and in the top part of Figure 3, an emissive signal is observed at position a, while at position b (Figure 3, bottom) an absorptive contribution at early time changes to an emissive signal at later time. The emissive signal at position a and the early absorptive contribution at position b are due to the radical pair $P_{700}^+A_1^-$, which dominates the spectra of the wild type (WT) in Figure 2 at 100 ns (solid curves). The emissive part of the transient at position b, on the other hand, is due to P_{700}^+ in the state $P_{700}^+FeS^-$, which gives rise to the spectra at 1.2 μs in Figure 2. Although it is known (*11*, *67*) that electron transfer from A_1 proceeds via F_X, we use FeS to represent one of the three iron−sulfur clusters and allow for the possibility that electron transfer from F_X to F_A/F_B is faster than from A_1 to F_X. Thus, the decay of the signals at position a and the transition from absorption to emission at position b are dominated by the rate of electron transfer from A_1^- to F_X. As is apparent, the transients at position a are all governed by the same lifetime, and fits of the data sets, which will be discussed below, yield an average value of 290 ns for the electron-transfer lifetime. The transients in the bottom part of Figure 3 are plotted with the same normalization as in the top part of the figure. Clearly, the relative amplitudes of the absorptive and emissive polarization differ significantly among the four samples isolated using Triton X-100 (Figure 2, left), while the four β-DM samples show much smaller changes. The differing intensities of the emissive polarization in the Triton X-100 samples are consistent with differing contributions from $P_{700}^+FeS^-$ at early time. Since the emissive contribution is strongest in the complexes isolated from the double mutant using Triton X-100, the results suggest that the combined effect of the mutations and Triton X-100 is to induce fast electron transfer to F_X in a significant fraction of the reaction centers. This is seen most clearly in the spectra in Figure 2, which show differing amounts of emissive polarization at early time in the Triton X-100 samples (Figure 2, left, solid curves). The most dramatic effect is found for the Δ*psaE*/Δ*psaF* double mutant, which has a completely emissive spectrum at 100 ns (Figure 2, bottom left, solid curve). The spectra at 1.2 μs also differ slightly among the Triton X-100 samples. In the wild type, this spectrum is almost purely emissive, while for the mutant samples an absorptive feature on the upfield end of the spectra is seen, which is again strongest in the Δ*psaE*/Δ*psaF* double mutant. There are several factors that could lead to such changes. The polarization of P_{700}^+ in the state $P_{700}^+FeS^-$ depends on the spin polarization pattern, lifetimes, relative orientations, and magnetic parameters of P_{700}^+, A_0^-, and A_1^-. For example, as discussed in ref *65*, an absorptive feature on the upfield end of the $P_{700}^+F_X^-$ spectrum can occur if singlet−triplet mixing takes place in the state $P_{700}^+A_0^-$. Such effects are also well-known in purple bacteria when the lifetime of $P_{865}^+I^-$ is increased (*34*−*36*). Possible changes in the features of the spectrum of $P_{700}^+A_1^-$ are difficult to study at room temperature because this requires separating the contributions from $P_{700}^+A_1^-$ and $P_{700}^+FeS^-$ in the data sets. Although this is possible using kinetic modeling (*11*), it is more convenient to measure the spectrum of $P_{700}^+A_1^-$ at low temperature, where no contribution from $P_{700}^+FeS^-$ is observed.

Low-Temperature Transient EPR Results. Figure 4 shows transient EPR spectra of the same samples taken at 135 K. Under these conditions the spectra are due to $P_{700}^+A_1^-$ in those reaction centers in which electron transfer past A_1 is blocked. Recent optical studies show that the fast component of electron transfer to F_X is independent of temperature in a minor fraction of reaction centers (*14*), suggesting that an electron-transfer cycle involving $P_{700}^+F_X^-$ may also occur to some extent under the conditions used for Figure 4. However, it has also been shown that the low-temperature transient EPR spectra of PS I from the wild type and from mutants lacking F_X, F_A, and F_B are identical (*68*). Hence, any contribution from $P_{700}^+FeS^-$ is negligible at low temperature. The comparison shown in Figure 4 reveals that the shape of the $P_{700}^+A_1^-$ spectra is also altered in the deletion mutant complexes isolated using Triton X-100 (Figure 4,

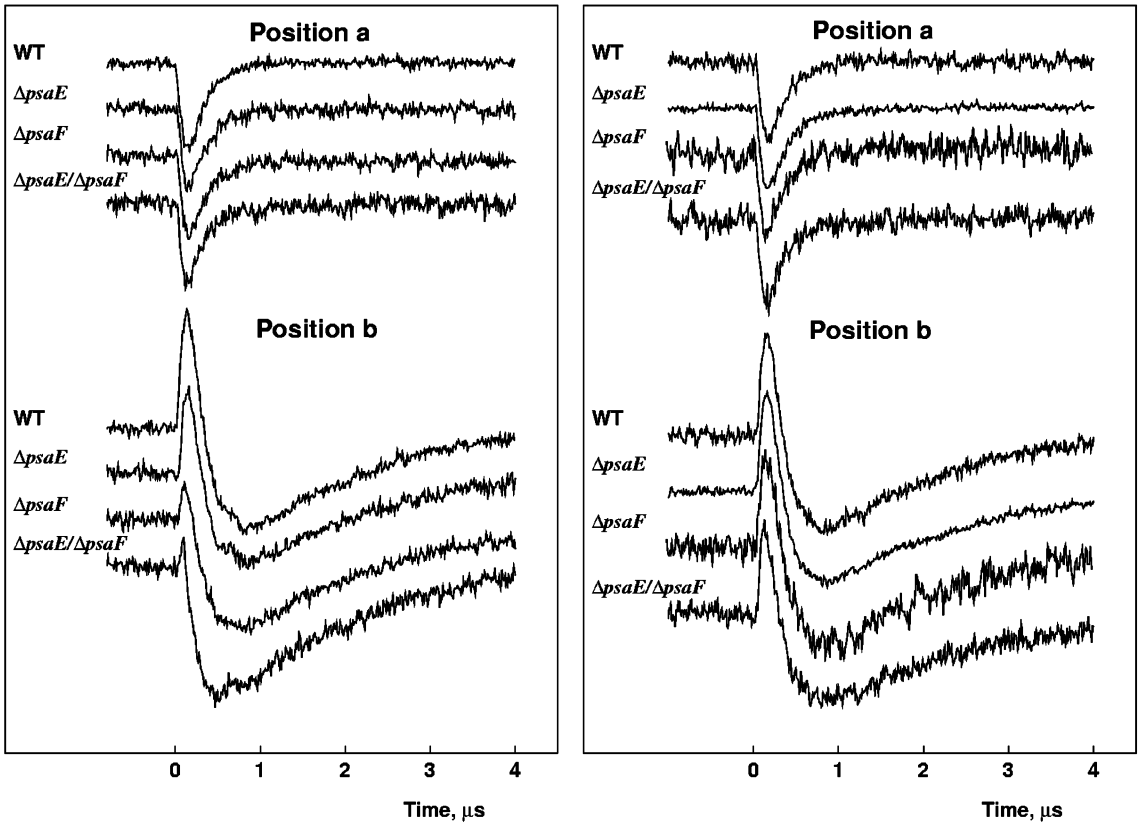

FIGURE 3: Comparison of EPR transients taken at the two different field positions indicated by the two arrow labels a and b in Figure 2. The transients taken at position a (top) are dominated by the A_1^- contribution to $P_{700}^+A_1^-$, while the transients at position b show an absorptive (positive) contribution from $P_{700}^+A_1^-$ at early times and an emissive signal (negative) due to $P_{700}^+FeS^-$ at later times. The traces on the left side of the figure are from PS I complexes isolated with Triton X-100, and those on the right are from complexes isolated with β-DM.

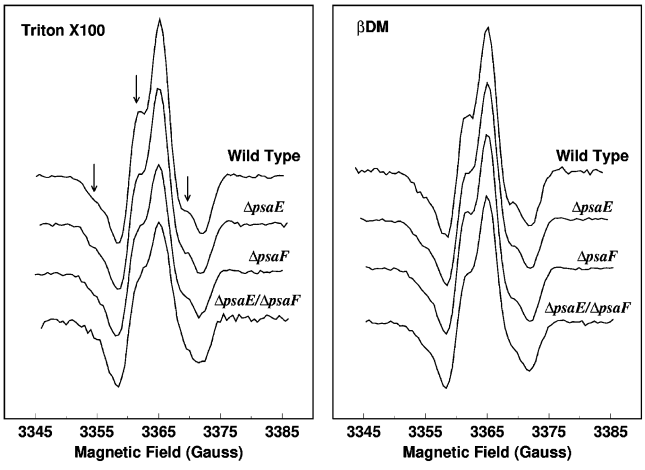

FIGURE 4: Spin-polarized transient EPR spectra of $P_{700}^+A_1^-$ at 135 K. The spectra are the integrated signal intensity taken in a time window from 0.4 to 0.8 μs after the laser flash. As in Figures 2 and 3, the spectra on the left of the figure are from PS I complexes isolated with Triton X-100 and those on the right are from complexes isolated with β-DM.

left). Similar changes are also observed in the β-DM samples (Figure 4, right), but they are much less pronounced. The main difference between the spectra of the wild-type and mutant PS I complexes is a change in the relative intensities of the emissive and absorptive features (see the discussion of Figure 5, below). In addition there is a small but reproducible loss of the shoulders (indicated by arrows in the wild-type spectrum) attributed to hyperfine coupling to the methyl group of the quinone. Recently, it has been shown that point mutations in the phylloquinone binding site in the PsaA branch affect the low-temperature spin polarization patterns in both green algae (*1*) and cyanobacteria (*5*) while the corresponding mutations in the PsaB branch do not, demonstrating that the quinone observed in low-temperature transient EPR experiments is in the PsaA branch. This quinone is bound via a single hydrogen bond to the backbone nitrogen of LeuA722, and the methyl substituent on the phylloquinone headgroup is *meta* to the H-bonded carbonyl (*69*). This asymmetric H-bonding arrangement distorts the spin density on the quinone such that it alternates around the quinone ring and is highest adjacent to the methyl group (*59*−*61*, *70*). Because of this, the methyl hyperfine coupling is unusually large (*40*, *52*, *71*) and is partially resolved in the spin polarization pattern (*25*, *59*−*61*). In the spectra of the mutants shown in Figure 4, the methyl hyperfine structure is not as well resolved, suggesting that the detergent may affect the strength of the hydrogen bond. LeuA722 is in a loop region of the protein on the stromal surface of the membrane but is shielded from the stroma by the peripheral subunits PsaE and PsaF. Thus, it is possible that, in the absence of one or both of these subunits, the detergent used to isolate PS I causes some conformational disorder in the loop region, leading to a distribution of hydrogen bond strengths and a distribution of methyl hyperfine couplings. Simulations (not shown) indicate that the loss of the shoulders in Figure 4 is consistent with a reduction of the methyl group hyperfine couplings. However, the strength of

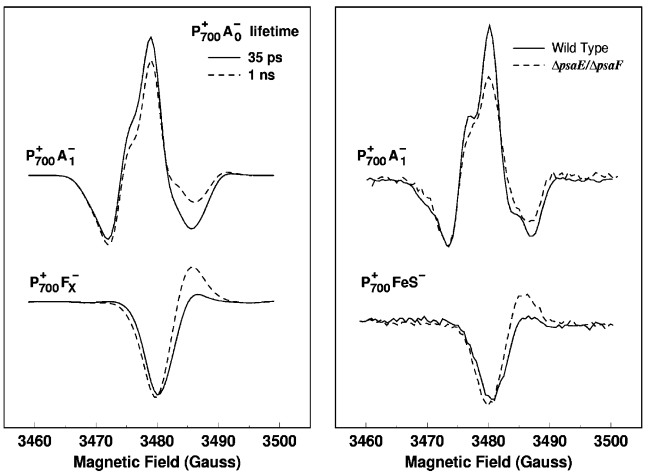

FIGURE 5: Left: Calculated spin-polarized EPR spectra of $P_{700}^+A_1^-$ (top) and $P_{700}^+F_X^-$ (bottom) for two different lifetimes for $P_{700}^+A_0^-$. Solid curves: $\tau = 35$ ps. Dashed curves: $\tau = 1$ ns. The spectra have been calculated as described in detail in refs *62* and *65* and take into account the spin dynamics in three sequential radial pairs. The magnetic and geometric parameters are given in ref *65* and have been taken from EPR experimental data and the X-ray structure. Right: Experimental spin-polarized EPR spectra of $P_{700}^+A_1^-$ (top) and $P_{700}^+FeS^-$ (bottom) of the wild type (solid curves) and the Δ*psaE*/Δ*psaF* mutant isolated with Triton X-100 (dashed curves). The spectra of $P_{700}^+A_1^-$ (top) are the signal intensity at 135 K in a time window centered at 0.6 μs after the laser flash, while the $P_{700}^+FeS^-$ spectra (bottom) are taken at room temperature in a window centered at 1.2 μs (dashed line) after the laser flash.

the coupling is difficult to assess accurately from the transient EPR spectra, and further studies (e.g., pulsed ENDOR measurements (*49*)) are required to confirm this hypothesis. The interaction between the subunits and possible structural changes will be discussed in more detail below.

As mentioned above, the appearance of an absorptive feature on the high-field side of the $P_{700}^+FeS^-$ spectrum at room temperature (Figure 2, dashed curves) is indicative of singlet−triplet mixing in the state $P_{700}^+A_0^-$ (*65*). If such mixing does indeed occur in the mutants, then it should also lead to changes in the spectra of the subsequent radical pairs $P_{700}^+A_1^-$ and $P_{700}^+F_X^-$. In general, any spin polarization pattern generated by spin dynamics can be broken down into "net" and "multiplet" contributions. The net contribution imparts a purely emissive or purely absorptive EPR signal to each spin, while the multiplet contribution gives each spin a signal which has equal amounts of absorption and emission. An extensive discussion of light-induced electron spin polarization is given in ref *72*, and its properties in photosynthetic reaction centers are reviewed in refs *20* and *25*. As discussed in ref *62*, under the conditions found in photosynthetic reaction centers, there are two additional contributions to the spin polarization induced by singlet−triplet mixing in a precursor. The first of these imparts a net polarization to each of the radicals in subsequent radical pairs (*29*). The strength of the polarization is given approximately by (*62*)

$$p = \frac{qb}{\Omega^2 + k^2} \tag{1}$$

where $\Omega^2 = q^2 + b^2$, q is the difference in the precession frequencies of the two spins (i.e., the frequency of the singlet−triplet mixing), $b = 2J + d$ is the flip-flop term of the spin−spin coupling, J is the exchange coupling, d is the dipolar coupling, and k is the mean decay rate for the precursor radical pair. In reaction centers of heliobacteria, green sulfur bacteria (*64*, *65*), and modified purple bacteria (*35*, *36*), this term produces net absorptive polarization of P^+ because both q and b are positive in the initial radical pair (*34*−*36*). Although the sign of b is not known with certainty for $P_{700}^+A_0^-$ in PS I, it is reasonable to assume that it is positive as in the other reaction centers. Thus, net absorptive polarization of P_{700}^+ is expected if the lifetime of $P_{700}^+A_0^-$ is sufficiently long. To analyze the spectrum of $P_{700}^+F_X^-$, the generation of the net polarization on both precursors $P_{700}^+A_0^-$ and $P_{700}^+A_1^-$ must be considered. The sign of b is opposite in $P_{700}^+A_0^-$ and $P_{700}^+A_1^-$ as a result of the difference in the relative magnitudes of J and d in the two radical pairs. Because of this, the contribution to the net polarization from spin dynamics in $P_{700}^+A_1^-$ is emissive. Hence, the overall net polarization of P_{700}^+ may be of either sign in $P_{700}^+F_X^-$ depending on the relative strengths of the absorptive and emissive contributions from the spin dynamics in $P_{700}^+A_0^-$ and $P_{700}^+A_1^-$, respectively. In native PS I, the lifetime of $P_{700}^+A_0^-$ is very short (∼35 ps) so that the emissive contribution from singlet−triplet mixing in $P_{700}^+A_1^-$ dominates the net polarization of P_{700}^+ in $P_{700}^+F_X^-$.

In addition to the net polarization, singlet−triplet mixing also causes multiplet polarization of the donor because of the inhomogeneous broadening from unresolved hyperfine coupling. This term only produces polarization of the donor because the hyperfine configurations in the two sequential acceptors are uncorrelated, which leads to cancellation of the multiplet polarization in the acceptor(s) (*26*). The polarization from this term is given by (*62*)

$$p = \frac{q\Delta}{\Omega^2 + k^2} \tag{2}$$

where Δ is the half-width of the Gaussian line shape describing inhomgeneous broadening. In PS I, q is positive and this term produces an E/A (E = emission, A = absorption) polarization pattern for P_{700}^+. To investigate the possibility that the changes in the experimental spectra are related to these effects, the spectra of $P_{700}^+A_1^-$ and $P_{700}^+F_X^-$ were calculated as a function of the lifetime of $P_{700}^+A_0^-$. An example of these calculations is shown on the left side of Figure 5. The solid curves correspond to a $P_{700}^+A_0^-$ lifetime of 35 ps, as has been estimated for wild-type PS I (*73*), while the dashed curves correspond to a lifetime of 1 ns. The magnetic and geometric parameters used for the calculations are summarized in Table 1 and have been taken from the literature. In cases in which several literature values exist, we have taken an average or chosen one of them. Although this remaining uncertainty in the parameters does have some effect on the calculated spectra, the parameters are sufficiently well established to allow a qualitative analysis of the effect of an increase in the lifetime of $P_{700}^+A_0^-$. As can be seen, the increase in the lifetime leads to the expected absorbance on the high-field end of the $P_{700}^+F_X^-$ spectrum (Figure 5, bottom left) and changes the shape of the $P_{700}^+A_1^-$ spectrum (Figure 5, top left). On the right side of Figure 5, the low-temperature spectra of $P_{700}^+A_1^-$ and the room temperature spectra of $P_{700}^+F_X^-$ in the wild type (solid

Table 1: Summary of Magnetic and Geometric Parameters Held Fixed in the Simulations

	g tensors			line widths	
	g_{xx}	g_{yy}	g_{zz}	(mT)	refs
P_{700}^+	2.0031	2.0026	2.0022	0.40	*61, 76−78*
A_0^-	2.0031	2.0031	2.0031	0.40	*16, 79, 80*
A_1^-	2.0063	2.0051	2.0022	0.18	*37, 38, 61*
F_X^-	1.78	1.86	2.06	2.0	81

A_1^- methyl hyperfine coupling (mT)			Euler angles (deg) between $g(A_1)$ and $A(CH_3)$			
A_{xx}	A_{yy}	A_{zz}	α	β	γ	refs
0.32	0.32	0.46	30	0	0	*49, 53, 61*

	Euler angles (deg) relating g tensors			dipolar axis in $g(P_{700})$		spin−spin coupling (mT)		
	α	β	γ	θ	φ	J	D	refs
$P_{700}^+ A_0^-$				17.9	153.2	0.5	−0.34	*65, 69*
$P_{700}^+ A_1^-$	2.0	126.0	81.0	34.5	78.7	0.0	−0.17	*44, 61, 65, 82*
$P_{700}^+ F_X^-$	180.0	131.1	70.6	59.7	65.4	0.0	−0.10	*65, 69*

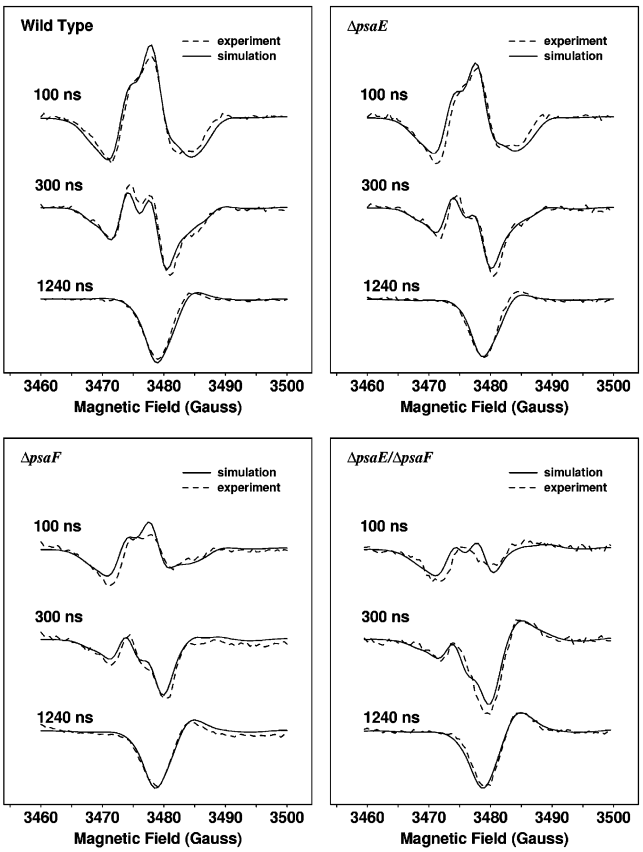

FIGURE 6: Experimental data (dashed lines) and simulations (solid lines) of the transient EPR data sets for the PS I complexes isolated with Triton X-100. Representative boxcar spectra are shown in three different time windows centered at the times indicated. The procedure used to calculate the simulated spectra is discussed in the text.

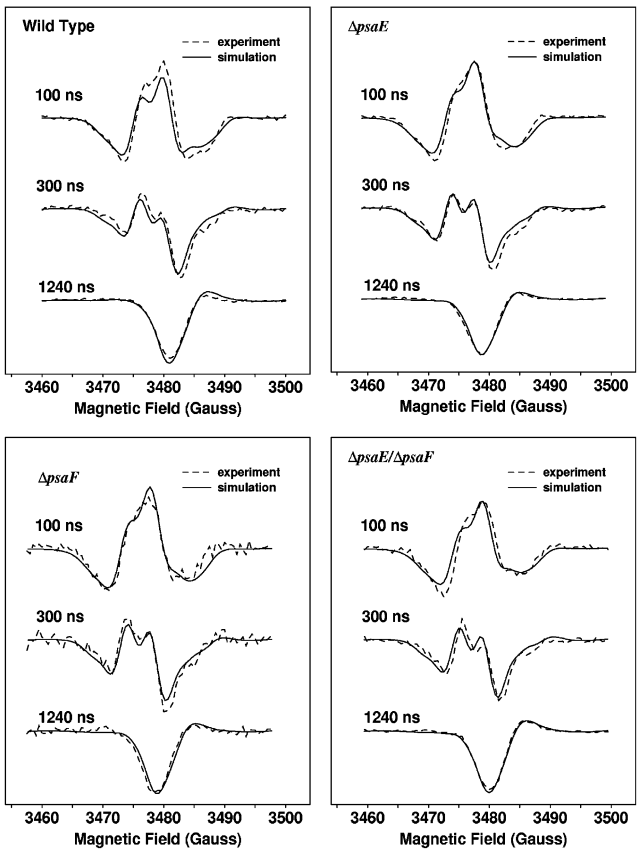

FIGURE 7: Experimental data (dashed lines) and simulations (solid lines) of the transient EPR data sets for the PS I complexes isolated with β-DM. Representative boxcar spectra are shown in three different time windows.

curves) and Δ*psaE*/Δ*psaF* mutant (dashed curves) are compared for Triton X-100 complexes. Clearly the changes in the experimental spectra resemble those in the simulations. Thus, it is likely that forward electron transfer from A_0^- to A_1 is also affected in the mutants, particularly when Triton X-100 is used in the isolation of PS I.

Analysis of Room Temperature Transient EPR Data. Figures 6 and 7 show the results of fits to the room temperature data sets based on a kinetic model in which two populations of reaction centers are assumed. The EPR signal as a function of field position and time is then given by

$$S(t,B_0) = (1 - X)S_1(t,B_0) + XS_2(t,B_0)$$

$$S_1(t,B_0) = \alpha(B_0)e^{-(k_1+w)t} + \beta(B_0)e^{-wt}(1 - e^{-k_1 t})$$

$$S_2(t,B_0) = \alpha'(B_0)e^{-(k_1'+w)t} + \beta'(B_0)e^{-wt}(1 - e^{-k_1' t}) \quad (3)$$

where k_1 and k_1' are the rates of electron transfer from A_1^- to F_X and X is the fraction of reaction centers in which the forward electron transfer is governed by k_1'. The rate of spin

Table 2: Kinetic Parameters and Amplitudes Obtained from Global Fits of the Transient EPR Data Sets[a]

detergent	sample	k^{-1} (ns)	w^{-1} (μs)	X
Triton X-100	WT	340	1.04	0.17
	Δ*psaE*	300	1.23	0.23
	Δ*psaF*	250	1.54	0.35
	Δ*psaE*/Δ*psaF*	210	1.38	0.55
Δ-DM	WT	290	1.25	0.17
	Δ*psaE*	320	1.25	0.20
	Δ*psaF*	320	1.27	0.19
	Δ*psaE*/Δ*psaF*	340	1.33	0.36

[a] The parameters *k*, *w*, and *X* are defined in eq 3.

relaxation is given by *w* and is assumed to be the same for all radical pairs. The spectra of $P_{700}^{+}A_1^{-}$ and $P_{700}^{+}F_X^{-}$ for the two fractions are represented by $\alpha(B_0)$, $\alpha'(B_0)$, $\beta(B_0)$, and $\beta'(B_0)$. Here, we calculate the spectra of these species and fit $S(t,B_0)$ to the time/field data sets with k_1, *w*, and *X* as free parameters. The rise time of the spectrometer and the lifetime broadening are taken into account by convoluting $S(t,B_0)$ with the spectrometer response function and a Lorentzian line shape, respectively. With these assumptions, we have separated the spectral dependence and time dependence of the data and have ignored coherent oscillations (*55*, *74*, *75*) of the spin system. We expect this approximation to be valid for times that are long compared to the lifetime of singlet−triplet mixing in the sequential radical pairs, i.e., times longer than ∼50 ns, but not for the short time behavior of the system. Thus, we can use this approach to reproduce the spectra at various times >50 ns and estimate the fraction of fast electron transfer. It is important to point out that the values of the parameters obtained from the fits can be expected to show trends in the data but the ratio of the two kinetic components will have a large uncertainty associated with it because of the assumptions involved.

For the fits shown in Figures 6 and 7, we have used the geometric and magnetic parameters given in Table 1 and have assumed that the two fractions have different electron-transfer kinetics. In one fraction (corresponding to S_1 in eq 3), the lifetime of A_0^{-} is assumed to be too short for significant singlet−triplet mixing to occur (i.e., <∼500 ps), and the lifetime of A_1^{-} (k_1) is an adjustable parameter, which we expect to yield values of ∼250 ns. In the second fraction, which corresponds to S_2 in eq 3 and *X* in Table 2, we arbitrarily assume that electron transfer from A_0^{-} to A_1 occurs with a lifetime of 1 ns. This is based on the fact that changes similar to those observed experimentally are expected for A_0^{-} lifetimes in this range. The second fraction is further assumed to correspond to the fast component of electron transfer from A_1^{-} to F_X with a lifetime of 10 ns. As can be seen in the two figures, the experimental spectra are reproduced very well by this procedure, and it yields lifetimes that are in good agreement with previously determined values (*11*). The values of the fitted parameters are given in Table 2. The fraction of fast electron transfer in the wild type is ∼20%, in reasonable agreement with the ∼25−30% determined optically (*4*, *14*), and the changes in the spectra are reproduced well by increasing the fraction of fast electron transfer. However, these values should be treated with caution because three of the lifetimes used are below the time resolution of the spectrometer, and we have arbitrarily assumed values for them. Fits with different assumed values for the lifetimes give different ratios of the two phases, but the overall trends remain the same. For example, smaller values of *X* are obtained if a shorter lifetime for A_0^{-} or a longer lifetime for A_1^{-} is assumed for this fraction. It is also unlikely that the reoxidation of A_1^{-} is strictly biphasic, but rather the two lifetimes are probably the major components in a distribution of lifetimes. Indeed, there is evidence for this from recent low-temperature optical studies (*14*). Thus, the fits give only a qualitative estimate of how the fast component changes. Despite these limitations, it is clear from the analysis that the fraction of fast electron transfer to F_X is increased by the combined effects of the mutations and detergent isolation and the effect is largest in the Δ*PsaE*/Δ*PsaF* mutant.

DISCUSSION

The results presented above show that isolation of PS I with Triton X-100 has a significant influence on electron transfer from A_1 to F_X when the PsaF subunit is absent, and this effect is enhanced when PsaE is also absent. This mirrors almost exactly the photoaccumulation experiments in PS I mutants, in which a population of A_0^{-} was photoaccumulated at the expense of A_1^{-} when the PsaF subunit was missing and Triton X-100 was employed, and this effect was similarly enhanced when PsaE was also absent (*16*). The larger fraction of fast electron transfer in the Triton X-100 preparations is also reminiscent of similar effects observed in spinach complexes (*8*). Indeed, the transient EPR data from spinach PS Iβ complexes (*25*) closely resemble those of the Triton X-100 complexes of the double mutant presented in Figures 1 and 2 (bottom left). As discussed above, the proposal that the biphasic reoxidation of A_1^{-} represents electron transfer in the two branches of cofactors implies that changes in the ratio of the two phases represent changes in the efficiency of electron transfer in the two branches. Indeed, this assumption is important to the interpretation of the spectroscopic data of samples with point mutations which are expected to alter the quantum yield of electron transfer, e.g., in the A_0 binding site or in the vicinity of P_{700}. The results presented here suggest that caution should be exercised in interpreting changes in the ratio of the two kinetic phases. The spectra in Figure 4, which are known to be associated with the PsaA branch quinone, are also altered, and there is evidence that forward electron transfer from A_0^{-} may also be slowed in the PsaA branch. Both of these effects are consistent with an alteration of the environment and properties of Q_K-A. That such changes should occur is not surprising given the locations of PsaE and PsaF on the stromal side of the PS I complex near the PsaA branch electron transport cofactors (Figure 1). The contacts between PsaF and other subunits of the PS I complex are listed in Table 3. As shown in the left column of Table 3, PsaF is hydrogen bonded to PsaA, PsaB, and PsaE. In the last two columns, the locations of the contacts within the complex are given. From this it is clear that the majority of the contacts are on the stromal side of the membrane, primarily in the A-jk(1) loop/helix region. A smaller series of contacts is also found in the B-gh loop region on the lumenal side of the membrane. However, these are well removed from the electron-transfer cofactors, which are bound via residues predominantly in helix j. Moreover, the changes in the electron-transfer kinetics are enhanced by removal of PsaE,

Table 3: Contacts between PsaF and Other PS I Subunits

subunit	residue	atom	PsaF residue	atom	distance (Å)	side	location
PsaA	Lys_{710}	O	Ala_{131}	N	3.02	stroma	A-jk(1) helix
PsaA	Lys_{710}	N^{ζ}	Asp_{133}	$O^{\delta 2}$	2.73	stroma	A-jk(1) helix
PsaA	Leu_{711}	O	Arg_{82}	N^{ϵ}	3.03	stroma	A-jk(1) helix
PsaA	Lys_{712}	O	Arg_{89}	$N^{\eta 1}$	3.08	stroma	A-jk(1) helix
PsaA	Lys_{712}	O	Arg_{89}	$N^{\eta 2}$	2.88	stroma	A-jk(1) helix
PsaA	Ala_{714}	O	Arg_{89}	$N^{\eta 2}$	3.16	stroma	A-jk(1) loop
PsaA	Ala_{716}	N	Glu_{98}	$O^{\epsilon 2}$	2.83	stroma	A-jk(1) loop
PsaA	Ile_{717}	N	Glu_{98}	$O^{\epsilon 1}$	2.99	stroma	A-jk(1) loop
PsaB	Arg_{548}	$N^{\eta 1}$	Arg_{141}	$O^{\xi t}$	2.76	stroma	B-h helix
PsaB	Glu_{419}	$O^{\epsilon 1}$	Arg_{141}	$N^{\eta 2}$	2.58	stroma	B-g helix
PsaB	Lys_{418}	N^{ζ}	Ser_{129}	O^{γ}	2.63	stroma	B-g-helix
PsaB	Gln_{416}	O	Arg_{141}	$N^{\eta 2}$	2.99	stroma	B-fg loop
PsaB	Lys_{551}	N^{ζ}	Thr_{137}	$O^{\gamma 1}$	3.16	stroma	B-hi loop
PsaB	Glu_{459}	N	Leu_{51}	O	3.28	lumen	B-gh loop
PsaB	Glu_{459}	$O^{\epsilon 2}$	His_{50}	$N^{\delta 1}$	2.40	lumen	B-gh loop
PsaB	Leu_{457}	O	Leu_{51}	N	2.79	lumen	B-gh loop
PsaB	Glu_{453}	$O^{\epsilon 1}$	Arg_{34}	N^{ϵ}	2.64	lumen	B-gh loop
PsaE	Pro_{12}	O	H_2O_{152}	O	3.11	stroma	
PsaE	H_2O_{152}	O	Val_{138}	O	3.12	stroma	
PsaE	Tyr_{17}	O	Thr_{37}	$O^{\gamma 1}$	2.83	stroma	

which is located on the stromal side of the complex. Thus, it is unlikely that changes near the contacts on the lumenal side of PS I are responsible for the observed effects. The contacts in the A-jk(1) loop/helix region are depicted in more detail in the top part of Figure 8, which shows a view roughly along the membrane normal. As enumerated in Table 3, PsaF is bound to PsaA through a series of eight hydrogen bonds to residues between $K710_{PsaA}$ and $I717_{PsaA}$. Thus, it appears that one of the roles of PsaF is to stabilize the structure of the A-jk(1) loop. This has obvious importance for electron transfer in PS I because the quinone in the PsaA branch (Q_K-A) is hydrogen bonded to the backbone nitrogen of $L722_{PsaA}$, which is located near the region in contact with PsaF. In the absence of PsaF, it is likely that conformational changes occur in the A-jk(1) loop, which in turn alter the properties of Q_K-A. The contacts to PsaE are also located in this region so that any conformational changes resulting from the loss of PsaF would be enhanced in the absence of PsaE. In ref *16*, it was postulated that the action of Triton X-100 was to open a water channel to the quinone, allowing it to be more easily protonated and doubly reduced. Such a pathway is apparent in the 2.5 Å crystal structure if one postulates that Triton X-100 is able to remove chlorophyll cofactors in this region when PsaF is missing. In the bottom part of Figure 8, the A-jk(1) loop region is shown roughly along the membrane plane. As can be seen, chlorophylls 1138 and 1139 are bound near the stromal surface in close proximity to both PsaF and the A-jk(1) loop. A series of tentatively identified water molecules are also shown, and it appears that the two chlorophylls shield Q_K-A from at least two of them. Since it is possible that Triton X-100 can extract one or both of the chlorophyll molecules in the absence of PsaF, this could expose Q_K-A to stromal water. Such changes would also be expected to influence the H-bonding between Q_K-A and $L722_{PsaA}$, which would be reflected in changes in the spin density distribution and the hyperfine couplings. Similarly, it is well-known that the redox potential of A_1 is strongly influenced by the surrounding protein so that changes in the binding of the quinone alter the electron-transfer kinetics. Indeed, this is the basis of the observations that point mutations in the A_1 binding site affect the electron-transfer

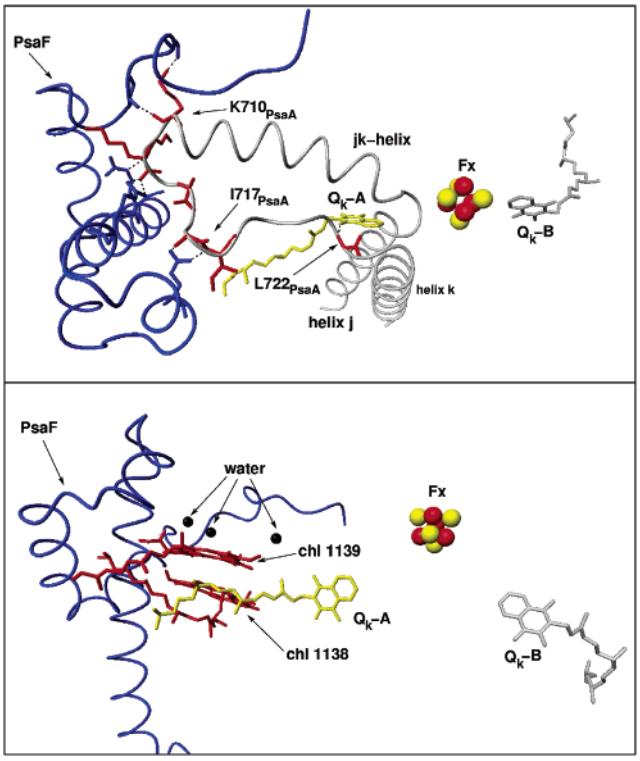

FIGURE 8: Structural features near PsaF on the stromal side of PS I from the 2.5 Å resolution X-ray structure (*69*) (PDB entry **1JB0**). Top: View of the A-jk(1) loop region from the stromal side of the membrane roughly along the membrane normal. H-bonding contacts between PsaA and PsaF are shown. Bottom: The same region is shown roughly parallel to the membrane plane. Two chlorophyll molecules (chl 1138 and chl 1139), which may be susceptible to solubilization in the absence of PsaF, are shown. The presence of water molecules on the stromal side of the chlorophylls suggests that Q_K-A would be exposed to water if these chlorophylls were extracted by Triton-X-100. The figure was constructed using the program MOLMOL (*83*).

kinetics. Although none of our data show conclusively in which branch the fast component of electron transfer induced by the absence of PsaF and Triton X-100-mediated changes occur, the most structurally reasonable explanation is that it is the PsaA branch. The alternative explanation that the change in the ratio of the fast and slow kinetic components results from a greater fraction of electron transfer in the PsaB branch would require that the initial ratio of charge separation is altered in the two branches. None of the contacts shown in Table 3 are close to P_{700} or A_0, and thus, it is difficult to see how changes associated with the absence of PsaF could influence the directionality. Moreover, this explanation would require that double reduction of the quinone in the PsaA branch takes place while photoaccumulation of A_1^- does not occur in the PsaB branch (*16*).

Recently an interesting alternative model for biphasic kinetic behavior was suggested (*14*) in which the electron transfer was proposed to proceed along the PsaB branch to F_X with a lifetime of 10 ns and then to either F_A/F_B or Q_K-A with a faster, unspecified lifetime. The slow phase of A_1^- reoxidation would then correspond to electron transfer from Q_k-A via F_X to F_A/F_B. Under this model a change in the ratio of the two phases would represent a change in the fraction of electrons being transferred from F_X^- to F_A/F_B or Q_K-A. Such a change would also be expected if the structural changes outlined above occurred. However, this model is

difficult to reconcile with the spin-polarized EPR data because the fast electron spin relaxation of F_X^- and spin evolution in the radical pair $P_{700}^+Q_K$-B^- should lead to $P_{700}^+Q_K$-A^- spectra which are different from those observed. Moreover, removal of F_X should also lead to changes in the spin polarization patterns, yet no such differences are seen (*68*).

Thus, the data presented here suggest that structural changes promoted by the removal of PsaF induce fast reoxidation of the quinone in the PsaA branch and that this effect is probably responsible for the changes in the ratio of the two kinetic phases in spinach preparations. However, it is important to point out that although this explanation of the detergent-induced effects is more in line with the unidirectional model, it does not rule out a bidirectional model in intact PS I.

REFERENCES

1. Boudreaux, B., MacMillan, F., Teutloff, C., Agalarov, R., Gu, F. F., Grimaldi, S., Bittl, R., Brettel, K., and Redding, K. (2001) Mutations in both sides of the Photosystem I reaction center identify the phylloquinone observed by electron paramagnetic resonance spectroscopy, *J. Biol. Chem. 276*, 37299−37306.
2. Guergova-Kuras, M., Boudreaux, B., Joliot, A., Joliot, P., and Redding, K. (2001) Evidence for two active branches for electron transfer in Photosystem I, *Proc. Natl. Acad. Sci. U.S.A. 98*, 4437−4442.
3. Muhiuddin, I. P., Heathcote, P., Carter, S., Purton, S., Rigby, S. E. J., and Evans, M. C. W. (2001) Evidence from time resolved studies of the $P_{700}^+A_1^-$ radical pair for photosynthetic electron transfer on both the PsaA and PsaB branches of the Photosystem I reaction centre, *FEBS Lett. 503*, 56−60.
4. Xu, W., Chitnis, P., Valieva, A., van der Est, A., Brettel, K., Guergova-Kuras, M., Pushkar, J., Zech, S., Stehlik, D., Shen, G., Zybailov, B., and Golbeck, J. (2003) Electron transfer in cyanobacterial Photosystem I. II. Determination of forward electron transfer rates of site-directed mutants in a putative electron transfer pathway from A_0 through A_1 to F_X, *J. Biol. Chem. 278*, 27876−27887.
5. Xu, W., Chitnis, P., Valieva, A., van der Est, A., Pushkar, J., Krzystyniak, M., Teutloff, C., Zech, S. G., Bittl, R., Stehlik, D., Zybailov, B., Shen, G., and Golbeck, J. (2003) Electron transfer in cyanobacterial Photosystem I. I. Physiological and spectroscopic characterization of site-directed mutants in a putative electron transfer pathway from A_0 through A_1 to F_X, *J. Biol. Chem. 278*, 27864−27875.
6. Brettel, K. (1997) Electron transfer and arrangement of the redox cofactors in Photosystem I, *Biochim. Biophys. Acta 1318*, 322−373.
7. Brettel, K., and Leibl, W. (2001) Electron transfer in Photosystem I, *Biochim. Biophys. Acta 1507*, 100−114.
8. Sétif, P., and Brettel, K. (1993) Forward electron transfer from phylloquinone A_1 to iron−sulfur centers in spinach Photosystem I, *Biochemistry 32*, 7846−7854.
9. Brettel, K. (1988) Electron transfer from A_1^- to an iron−sulfur center with $t_{1/2}$ = 200ns at room temperature in Photosystem I, *FEBS Lett. 239*, 93−98.
10. Bock, C. H., van der Est, A. J., Brettel, K., and Stehlik, D. (1989) Nanosecond electron transfer kinetics in Photosystem I as obtained from transient EPR at room temperature, *FEBS Lett. 247*, 91−96.
11. van der Est, A., Bock, C., Golbeck, J., Brettel, K., Sétif, P., and Stehlik, D. (1994) Electron transfer from acceptor A_1 to the iron−sulfur centers in Photosystem I as studied by transient EPR spectroscopy, *Biochemistry 33*, 11789−11797.
12. Brettel, K. (1999) Electron transfer from acceptor A_1 to the iron−sulfur clusters in Photosystem I measured with a time resolution of 2 ns, in *Photosynthesis, Mechanisms and Effects* (Garab, G., Ed.) pp 611−614, Kluwer Academic, Dordrecht, The Netherlands.
13. Schlodder, E., Falkenberg, K., Gergeleit, M., and Brettel, K. (1998) Temperature dependence of forward and reverse electron transfer from A_1^-, the reduced secondary electron acceptor in Photosystem I, *Biochemistry 37*, 9466−9476.
14. Agalarov, R., and Brettel, K. (2003) Temperature dependence of biphasic forward electron transfer from the phylloquinone(s) A_1 in Photosystem I: only the slower phase is activated, *Biochim. Biophys. Acta, Bioenerg. 1604*, 7−12.
15. Jolliot, P., and Jolliot, A. (1999) In vivo analysis of the electron transfer within Photosystem I: Are the two phylloquinones Involved? *Biochemistry 38*, 11130−11136.
16. Yang, F., Shen, G. Z., Schluchter, W. M., Zybailov, B. L., Ganago, A. O., Vassiliev, I. R., Bryant, D. A., and Golbeck, J. H. (1998) Deletion of the PsaF polypeptide modifies the environment of the redox-active phylloquinone A_1. Evidence for unidirectionality of electron transfer in Photosystem I, *J. Phys. Chem. B 102*, 8288−8299.
17. Schubert, W. D., Klukas, O., Krauss, N., Saenger, W., Fromme, P., and Witt, H. T. (1997) Photosystem I of *Synechococcus elongatus* at 4 Å resolution: comprehensive structure analysis, *J. Mol. Biol. 272*, 741−769.
18. Lagoutte, B., Sétif, P., and Duranton, J. (1984) Tentative identification of the apoproteins of iron−sulfur centers of Photosystem I, *FEBS Lett. 174*, 24−29.
19. Hoff, A. (1993) In *The Photosynthetic Reaction Center* (Deisenhofer, J., and Norris, J. R., Eds.) pp 331−386, Academic Press, San Diego/London.
20. Snyder, S. W., and Thurnauer, M. (1993) In *The Photosynthetic Reaction Center* (Deisenhofer, J., and Norris, J. R., Eds.) pp 285−330, Academic Press, San Diego/London.
21. Angerhofer, A., and Bittl, R. (1996) Radicals and radical pairs in photosynthesis, *Photochem. Photobiol. 63*, 11−38.
22. Möbius, K. (2001) High-field and high-frequency electron paramagnetic resonance, *Appl. Magn. Reson. 21*, 255−255.
23. Möbius, K. (2000) Primary processes in photosynthesis: what do we learn from high-field EPR spectroscopy? *Chem. Soc. Rev. 29*, 129−139.
24. Stehlik, D., and Möbius, K. (1997) New EPR methods for investigating photoprocesses with paramagnetic intermediates, *Annu. Rev. Phys. Chem. 48*, 745−784.
25. van der Est, A. (2001) Light-induced spin polarization in type I photosynthetic reaction centres, *Biochim. Biophys. Acta 1507*, 212−225.
26. Pedersen, J. B. (1979) Determination of the primary reactions of photosynthesis from transient ESR signals, *FEBS Lett. 97*, 305−310.
27. Norris, J. R., Morris, A. L., Thurnauer, M. C., and Tang, J. (1990) A general model of electron-spin polarization arising from the interactions within radical pairs, *J. Chem. Phys. 92*, 4239−4249.
28. Morris, A. L., Snyder, S. W., Zhang, Y. N., Tang, J., Thurnauer, M. C., Dutton, P. L., Robertson, D. E., and Gunner, M. R. (1995) Electron-spin polarization model applied to sequential electron-transfer in iron-containing photosynthetic bacterial reaction centers with different quinones as Q_A, *J. Phys. Chem. 99*, 3854−3866.
29. Hore, P. J. (1996) Transfer of spin correlation between radical pairs in the initial steps of photosynthetic energy conversion, *Mol. Phys. 89*, 1195−1202.
30. Kandrashkin, Y. E., Salikhov, K. M., and Stehlik, D. (1997) Spin dynamics and EPR spectra of consecutive spin-correlated radical pairs. Model calculations, *Appl. Magn. Reson. 12*, 141−166.
31. Snyder, S. W., Morris, A. L., Bondeson, S. R., Norris, J. R., and Thurnauer, M. C. (1993) Electron-spin polarization in sequential electron transfer—an example from iron-containing photosynthetic bacterial reaction center proteins, *J. Am. Chem. Soc. 115*, 3774−3775.
32. Utschig, L. M., Greenfield, S. R., Tang, J., Laible, P. D., and Thurnauer, M. C. (1997) Influence of iron-removal procedures on sequential electron transfer in photosynthetic bacterial reaction centers studied by transient EPR spectroscopy, *Biochemistry 36*, 8548−8558.
33. Tang, J., Bondeson, S., and Thurnauer, M. C. (1996) Effects of sequential electron transfer on electron spin polarized transient EPR spectra at high fields, *Chem. Phys. Lett. 253*, 293−298.
34. Tang, J., Utschig, L. M., Poluektov, O., and Thurnauer, M. C. (1999) Transient W-band EPR study of sequential electron transfer in photosynthetic bacterial reaction centers, *J. Phys. Chem. B 103*, 5145−5150.
35. Hulsebosch, R. J., Borovykh, I. V., Paschenko, S. V., Gast, P., and Hoff, A. J. (1999) Radical pair dynamics and interactions in quinone-reconstituted photosynthetic reaction centers of *Rb. sphaeroides* R26: A multifrequency magnetic resonance study, *J. Phys. Chem. B 103*, 6815−6823.

36. Hulsebosch, R. J., Borovykh, I. V., Paschenko, S. V., Gast, P., and Hoff, A. (2001) Erratum: radical pair dynamics and interactions in quinone-reconstituted photosynthetic reaction centers of *Rb. Sphaeroides* R26: A multifrequency magnetic resonance study, *J. Phys. Chem. B 105*, 10146.
37. van der Est, A., Prisner, T., Bittl, R., Fromme, P., Lubitz, W., Möbius, K., and Stehlik, D. (1997) Time-resolved X-, K-, and W-band EPR of the radical pair state $P_{700}^{+}A_1^{-}$ of Photosystem I in comparison with $P_{865}^{+}Q_A^{-}$ in bacterial reaction centers, *J. Phys. Chem. B 101*, 1437−1443.
38. MacMillan, F., Hanley, J., van der Weerd, L., Knupling, M., Un, S., and Rutherford, A. W. (1997) Orientation of the phylloquinone electron acceptor anion radical in Photosystem I, *Biochemistry 36*, 9297−9303.
39. Berthold, T., Bechtold, M., Heinen, U., Link, G., Poluektov, O., Utschig, L., Tang, J., Thurnauer, M. C., and Kothe, G. (1999) Magnetic-field-induced orientation of photosynthetic reaction centers as revealed by time-resolved W-band EPR of spin-correlated radical pairs, *J. Phys. Chem. B 103*, 10733−10736.
40. Teutloff, C., Hofbauer, W., Zech, S. G., Stein, M., Bittl, R., and Lubitz, W. (2001) High-frequency EPR studies on cofactor radicals in Photosystem I, *Appl. Magn. Reson. 21*, 363−379.
41. Fuhs, M., Schnegg, A., Prisner, T., Kohne, I., Hanley, J., Rutherford, A. W., and Möbius, K. (2002) Orientation selection in photosynthetic PS I multilayers: structural investigation of the charge separated state $P_{700}^{+}A_1^{-}$ by high-field/high-frequency time-resolved EPR at 3.4 T/95 GHz, *Biochim. Biophys. Acta 1556*, 81−88.
42. Zech, S. G., Lubitz, W., and Bittl, R. (1996) Pulsed EPR experiments on radical pairs in photosynthesis: Comparison of the donor−acceptor distances in Photosystem I and bacterial reaction centers, *Ber. Bunsen-Ges. Phys. Chem. 100*, 2041−2044.
43. Bittl, R., Zech, S. G., Fromme, P., Witt, H. T., and Lubitz, W. (1997) Pulsed EPR structure analysis of photosystem I single crystals: localization of the phylloquinone acceptor, *Biochemistry 36*, 12001−12004.
44. Zech, S. G., van der Est, A. J., and Bittl, R. (1997) Measurement of cofactor distances between P_{700}^{+} and A_1^{-} in native and quinone-substituted Photosystem I using pulsed electron paramagnetic resonance spectroscopy, *Biochemistry 36*, 9774−9779.
45. Bittl, R., and Zech, S. G. (1997) Pulsed EPR study of spin-coupled radical pairs in photosynthetic reaction centers: Measurement of the distance between P_{700}^{+} and A_1^{-} in Photosystem I and between P_{865}^{+} and Q_A^{-} in bacterial reaction centers, *J. Phys. Chem. B 101*, 1429−1436.
46. Dzuba, S. A., Hara, H., Kawamori, A., Iwaki, M., Itoh, S., and Tsvetkov, Y. D. (1997) Electron spin echo of spin-polarised radical pairs in intact and quinone-reconstituted plant Photosystem I reaction centres, *Chem. Phys. Lett. 264*, 238−244.
47. Iwaki, M., Itoh, S., Hara, H., and Kawamori, A. (1998) Spin-polarized radical pair in Photosystem I reaction center that contains different quinones and fluorenones as the secondary electron acceptor, *J. Phys. Chem. B 102*, 10440−10445.
48. Bittl, R., and Zech, S. G. (2001) Pulsed EPR spectroscopy on short-lived intermediates in photosystem I, *Biochim. Biophys. Acta 1507*, 194−211.
49. Fursman, C. E., Teutloff, C., and Bittl, R. (2002) Pulsed ENDOR studies of short-lived spin-correlated radical pairs in photosynthetic reaction centers, *J. Phys. Chem. B 106*, 9679−9686.
50. Käss, H., Fromme, P., Witt, H. T., and Lubitz, W. (2001) Orientation and electronic structure of the primary donor radical cation P_{700}^{+} in Photosystem I: A single crystals EPR and ENDOR study, *J. Phys. Chem. B 105*, 1225−1239.
51. Mino, H., Kawamori, A., Itoh, K., Miyamoto, R., and Itoh, S. (2003) Pulsed ENDOR study of spin-correlated radical pair in Photosystem I, *Plant Cell Physiol. 44*, S156−S156.
52. Muhiuddin, I. P., Rigby, S. E. J., Evans, M. C. W., Amesz, J., and Heathcote, P. (1999) ENDOR and special TRIPLE resonance spectroscopy of photoaccumulated semiquinone electron acceptors in the reaction centers of green sulfur bacteria and heliobacteria, *Biochemistry 38*, 7159−7167.
53. Rigby, S. E. J., Evans, M. C. W., and Heathcote, P. (1996) ENDOR and special triple resonance spectroscopy of A_1^{-} of Photosystem I, *Biochemistry 35*, 6651−6656.
54. Rigby, S. E. J., Evans, M. C. W., and Heathcote, P. (2001) Electron nuclear double resonance (ENDOR) spectroscopy of radicals in Photosystem I and related Type 1 photosynthetic reaction centres, *Biochim. Biophys. Acta 1507*, 247−259.
55. Kothe, G., Weber, S., Bittl, R., Ohmes, E., Thurnauer, M. C., and Norris, J. R. (1991) Transient EPR of light-induced radical pairs in plant Photosystem-I—observation of quantum beats, *Chem. Phys. Lett. 186*, 474−480.
56. Weber, S., Ohmes, E., Thurnauer, M. C., Norris, J. R., and Kothe, G. (1995) Light-generated nuclear quantum beats—a signature of photosynthesis, *Proc. Natl. Acad. Sci. U.S.A. 92*, 7789−7793.
57. Kamlowski, A., van der Est, A., Fromme, P., and Stehlik, D. (1997) Low temperature EPR on Photosystem I single crystals: Orientation of the iron−sulfur centers F_A and F_B, *Biochim. Biophys. Acta, Bioenerg. 1319*, 185−198.
58. Kamlowski, A., van der Est, A., Fromme, P., Krauss, N., Schubert, W. D., Klukas, O., and Stehlik, D. (1997) The structural organization of the PsaC protein in Photosystem I from single crystal EPR and X-ray crystallographic studies, *Biochim. Biophys. Acta 1319*, 199−213.
59. Kamlowski, A., Zech, S. G., Fromme, P., Bittl, R., Lubitz, W., Witt, H. T., and Stehlik, D. (1998) The radical pair state $P_{700}^{+}A_1^{-}$ in Photosystem I single crystals: Orientation dependence of the transient spin-polarized EPR spectra, *J. Phys. Chem. B 102*, 8266−8277.
60. Kamlowski, A., Altenberg-Greulich, B., van der Est, A., Zech, S. G., Bittl, R., Fromme, P., Lubitz, W., and Stehlik, D. (1998) The quinone acceptor A_1 in Photosystem I: Binding site, and comparison to Q_A in purple bacteria reaction centers, *J. Phys. Chem. B 102*, 8278−8287.
61. Zech, S. G., Hofbauer, W., Kamlowski, A., Fromme, P., Stehlik, D., Lubitz, W., and Bittl, R. (2000) A structural model for the charge separated state $P_{700}^{+}A_1^{-}$ in Photosystem I from the orientation of the magnetic interaction tensors, *J. Phys. Chem. B 104*, 9728−9739.
62. Kandrashkin, Y. E., Salikhov, K. M., van der Est, A., and Stehlik, D. (1998) Electron spin polarization in consecutive spin-correlated radical pairs: Application to short-lived and long-lived precursors in type 1 photosynthetic reaction centres, *Appl. Magn. Reson. 15*, 417−447.
63. Kandrashkin, Y., and van der Est, A. (2002) Electron spin polarization in photosynthetic reaction centres: Strategies for extracting structural and functional information, *Riken Rev. 44*, 124−127.
64. van der Est, A., Hager-Braun, C., Leibl, W., Hauska, G., and Stehlik, D. (1998) Transient electron paramagnetic resonance spectroscopy on green-sulfur bacteria and heliobacteria at two microwave frequencies, *Biochim. Biophys. Acta, Bioenerg. 1409*, 87−98.
65. Kandrashkin, Y. E., Vollmann, W., Stehlik, D., Salikhov, K., and van der Est, A. (2002) The magnetic field dependence of the electron spin polarization in consecutive spin correlated radical pairs in type I photosynthetic reaction centres, *Mol. Phys. 100*, 1431−1443.
66. Sakuragi, Y., Zybailov, B., Shen, G. Z., Jones, A. D., Chitnis, P. R., van der Est, A., Bittl, R., Zech, S., Stehlik, D., Golbeck, J. H., and Bryant, D. A. (2002) Insertional inactivation of the *menG* gene, encoding 2-phytyl- 1,4-naphthoquinone methyltransferase of *Synechocystis* sp PCC 6803, results in the incorporation of 2-phytyl-1,4-naphthoquinone into the A_1 site and alteration of the equilibrium constant between A_1 and F_x in Photosystem I, *Biochemistry 41*, 394−405.
67. Moenne Loccoz, P., Heathcote, P., Maclachlan, D. J., Berry, M. C., Davis, I. H., and Evans, M. C. W. (1994) Path of electron transfer in Photosystem 1—Direct evidence of forward electron transfer from A_1 to Fe−S_x, *Biochemistry 33*, 10037−10042.
68. Shen, G. Z., Antonkine, M. L., van der Est, A., Vassiliev, I. R., Brettel, K., Bittl, R., Zech, S. G., Zhao, J. D., Stehlik, D., Bryant, D. A., and Golbeck, J. H. (2002) Assembly of Photosystem I. II. Rubredoxin is required for the in vivo assembly of F_x in *Synechococcus* sp PCC 7002 as shown by optical and EPR spectroscopy, *J. Biol. Chem. 277*, 20355−20366.
69. Jordan, P., Fromme, P., Witt, H. T., Klukas, O., Saenger, W., and Krauss, N. (2001) Three-dimensional structure of cyanobacterial Photosystem I at 2.5 angstrom resolution, *Nature 411*, 909−917.
70. O'Malley, P. J. (1999) Density functional calculated spin densities and hyperfine couplings for hydrogen bonded 1,4-naphthosemiquinone and phyllosemiquinone anion radicals: a model for the A_1 free radical formed in Photosystem I, *Biochim. Biophys. Acta 1411*, 101−113.
71. Fursman, C. E., Bittl, R., Zech, S. G., and Hore, P. J. (2001) 95 GHz ESEEM of radical pairs: a source of radical separations and relative orientations, *Chem. Phys. Lett. 342*, 162−168.

72. Salikhov, K. M., Molin, Y. N., Sagdeev, R. Z., and Buchachenko, A. L. (1984) *Spin polarization and magnetic effects in radical reactions*, Elsevier, Amsterdam.
73. Brettel, K., and Vos, M. H. (1999) Spectroscopic resolution of the picosecond reduction kinetics of the secondary electron acceptor A_1 in Photosystem I, *FEBS Lett. 447*, 315−317.
74. Bittl, R., and Kothe, G. (1991) Transient EPR of radical pairs in photosynthetic reaction centers—Prediction of quantum beats, *Chem. Phys. Lett. 177*, 547−553.
75. Weber, S., Berthold, T., Ohmes, E., Thurnauer, M. C., Norris, J. R., and Kothe, G. (1996) Nuclear coherences in photosynthetic reaction centers following light excitation, *Appl. Magn. Reson. 11*, 461−469.
76. Poluektov, O. G., Utschig, L. M., Schlesselman, S. L., Lakshmi, K. V., Brudvig, G. W., Kothe, G., and Thurnauer, M. C. (2002) Electronic structure of the P_{700} special pair from high-frequency electron paramagnetic resonance spectroscopy, *J. Phys. Chem. B 106*, 8911−8916.
77. Prisner, T. F., McDermott, A. E., Un, S., Norris, J. R., Thurnauer, M. C., and Griffin, R. G. (1993) Measurement of the G-tensor of the P_{700}^+ signal from deuterated cyanobacterial Photosystem I particles, *Proc. Natl. Acad. Sci. U.S.A. 90*, 9485−9488.
78. Bratt, P. J., Rohrer, M., Krzystek, J., Evans, M. C. W., Brunel, L. C., and Angerhofer, A. (1997) Submillimeter high-field EPR studies of the primary donor in plant Photosystem I P_{700}, *J. Phys. Chem. B 101*, 9686−9689.
79. McCracken, J. L., and Sauer, K. (1983) Orientation dependence of radical pair interactions in spinach chloroplasts, *Biochim. Biophys. Acta 724*, 83−93.
80. Bonnerjea, J., and Evans, M. C. W. (1982) Identification of multiple components in the intermediary electron carrier complex of Photosystem I, *FEBS Lett. 148*, 313−316.
81. Guigliarelli, B., Guillaussier, J., More, C., Sétif, P., Bottin, H., and Bertrand, P. (1993) Structural organization of the iron−sulfur centers in *Synechocystis* 6803 Photosystem I. EPR study of oriented thylakoid membranes and analysis of the magnetic interactions, *J. Biol. Chem. 268*, 900−8.
82. Link, G., Berthold, T., Bechtold, M., Weidner, J. U., Ohmes, E., Tang, J., Poluektov, O., Utschig, L., Schlesselman, S. L., Thurnauer, M. C., and Kothe, G. (2001) Structure of the $P_{700}^+A_1^-$ radical pair intermediate in Photosystem I by high time resolution multifrequency electron paramagnetic resonance: Analysis of quantum beat oscillations, *J. Am. Chem. Soc. 123*, 4211−4222.
83. Koradi, R., Billeter, M., and Wuthrich, K. (1996) MOLMOL: a program for display and analysis of macromolecular structures, *J. Mol. Graphics 14*, 51−5, 29−32.

BI035431J